

## Supporting Information

---

### A Twisted Bi-icosahedral Au<sub>25</sub> Cluster Enclosed by Bulky Arenethiolates

Jun-ichi Nishigaki,<sup>1</sup> Seiji Yamazoe,<sup>1,2</sup> Shinji Kohara,<sup>3</sup> Akihiko Fujiwara,<sup>3</sup>  
Wataru Kurashige,<sup>4</sup> Yuichi Negishi,<sup>4</sup> and Tatsuya Tsukuda<sup>1,2\*</sup>

<sup>1</sup> Department of Chemistry, School of Science, The University of Tokyo, 7-3-1 Hongo, Bunkyo-ku, Tokyo 113-0033

<sup>2</sup> Elements Strategy Initiative for Catalysts and Batteries (ESICB), Kyoto University, Katsura, Kyoto 615-8520

<sup>3</sup> Japan Synchrotron Radiation Research Institute/ SPring-8, 1-1-1 Kouto, Sayo-cho, Sayo-gun, Hyogo 679-5198, Japan

<sup>4</sup> Department of Applied Chemistry, Faculty of Science, Tokyo University of Science, 1-3 Kagurazaka, Shinjuku-ku, Tokyo 162-8601

---

## 1. Experiment

### A. Synthesis

#### (i) General procedures

All reactions and manipulations of moisture-sensitive compounds were conducted under an inert atmosphere of dry argon employing standard Schlenk techniques. Milli-Q grade water was used in the present study. The reagents and solvents used were commercially available and used without further purification.

#### (ii) Synthesis of DppSH

2,6-Diphenylbenzenethiol (DppSH) was synthesized according to a slightly modified literature procedure<sup>1</sup> and characterized by <sup>1</sup>H NMR.

#### (iii) Synthesis of Au:SDpp

PVP-stabilized Au clusters (Au:PVP) were prepared by the batch mixing of HAuCl<sub>4</sub> and PVP (average molecular weight = 40 kDa, (K-30)) at 0 °C and ultracentrifuged (MWCO 10,000 Da membrane filter) to remove salts.<sup>2</sup> A brown hydrosol of Au:PVP (0.4 mM, 20 mL) was added to a toluene solution (8.0 mM, 20 mL) of DppSH and the mixture was stirred at 50 °C for 30 min. The resulting toluene solution was separated from the water layer and stirred at 80 °C for 12 h. After the solvent had evaporated, the brown residue was thoroughly washed by hexane to give a brown powder of Au<sub>25</sub>(SDpp)<sub>11</sub>. Au<sub>25</sub>(SDpp)<sub>11</sub> did not decompose during storage at -20 °C for several weeks.

### B. Characterization

#### (i) <sup>1</sup>H NMR measurements

<sup>1</sup>H NMR (400 MHz) spectra were recorded on a JEOL ECX-400 instrument using CDCl<sub>3</sub> as the solvent. The signals were referenced to the TMS and residual peak of deuterated solvents.

## **(ii) Optical absorption spectroscopy**

UV-vis spectra were recorded in a 10-mm quartz cell using a JASCO V-670 spectrophotometer. The samples were dissolved in toluene for the measurements. In order to optimize the extraction conditions of Au clusters, the yields under different conditions were monitored by absorbance of the extracted clusters at 400 nm. We found that Au clusters were completely extracted by 20 eq. excess DppSH at 50 °C for 30 min, in which no Au cluster was detected in the water phase. We used this yield (absorbance) as standard (~100%).

## **(iii) Matrix assisted laser desorption ionization (MALDI) mass spectrometry**

Low-resolution MALDI-TOF mass spectra were recorded using a time-of-flight mass spectrometer (Shimadzu Axima-CFR) operated with a N<sub>2</sub> laser (337 nm) for all spectra. The high-resolution MALDI-TOF mass spectra were recorded using a JEOL JMS-S3000 operated with a Nd:YAG laser (349 nm). Positive- and negative-ion mass spectra were recorded with a delayed extraction mode. Samples for mass analysis were prepared by mixing Au:SDpp and trans-2-[3-(4-tert-butylphenyl)-2-methyl-2-propenylidene]-malononitrile (DCTB)<sup>3</sup> with a typical molar ratio of 1:200.

## **(iv) Transmission electron microscopy (TEM)**

TEM images were captured using a Hitachi HF-2000 microscope operating at 200 kV. The toluene solution of Au<sub>25</sub>(SDpp)<sub>11</sub> was dropcast onto a hydrophobic carbon-coated copper grid followed by drying in vacuo.

## **(v) Fourier transformed infrared (FT-IR) spectroscopy**

FT-IR spectra were taken on a JASCO FT/IR-4200 spectrophotometer with samples prepared as KBr pellets.

## **(vi) High-energy X-ray diffraction**

High-energy X-ray diffraction (HEXRD) data were taken at the BL04B2 beamline at the SPring-8 facility of the Japan Synchrotron Radiation Research Institute. The energy of the incident X-rays was 37.6 keV. The vacuum dried Au<sub>25</sub>(SDpp)<sub>11</sub> powder was encapsulated in a thin-walled (thickness 0.01 mm) silica glass tube of 2 mm diameter. The raw data were corrected for polarization, absorption, and background from a silica glass tube, and the contribution of Compton scattering was subtracted using standard analysis procedures.<sup>4</sup> The corrected data sets were normalized to give the Faber-Ziman<sup>5</sup> total structure factor  $S(Q)$ , and the total correlation function  $T(r)$  was obtained by a Fourier transformation of  $S(Q)$ .

## 2. Results

### A. Characterization of DppSH

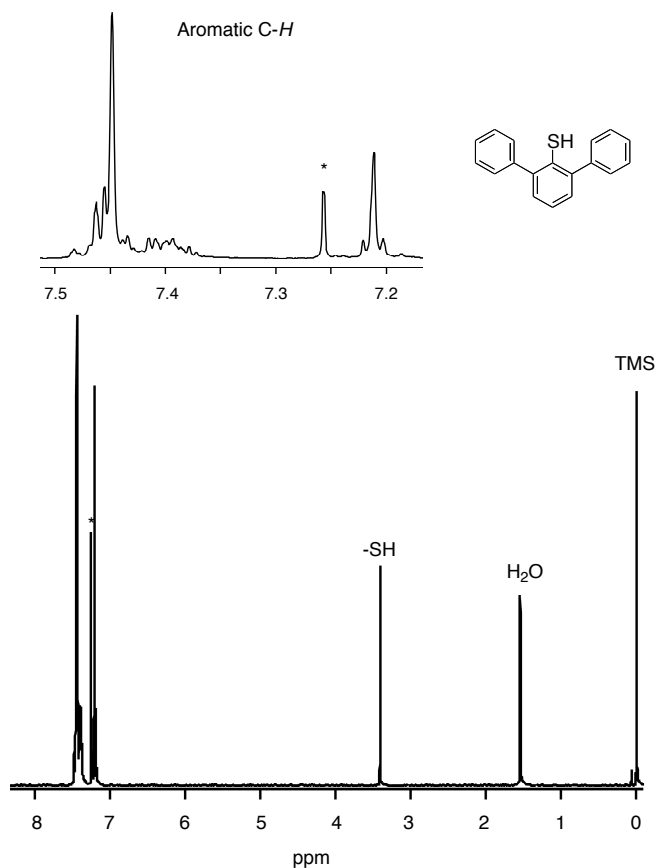


**Figure S1.** <sup>1</sup>H NMR spectrum of DppSH (CDCl<sub>3</sub>):  $\delta$  3.41 (s, 1 H, SH), 7.20-7.22 (m, 3 H, Ar), 7.37-7.48 (m, 10 H, Ar). The asterisk marks the residual proton peak of the solvent.

### B. Extraction efficiency under various conditions

#### (i) Concentration dependence of DppSH

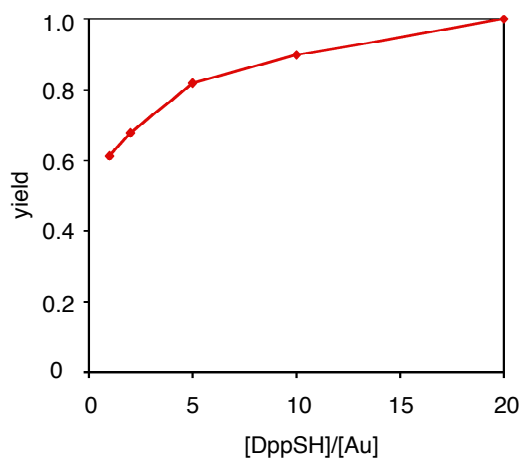


**Figure S2.** The yields of Au:SDpp for the ligand exchange reaction with various [DppSH]/[Au] ratios. The reactions proceeded at 50 °C for 30 min, [Au] = 0.4 mM.

### (ii) Temperature dependence

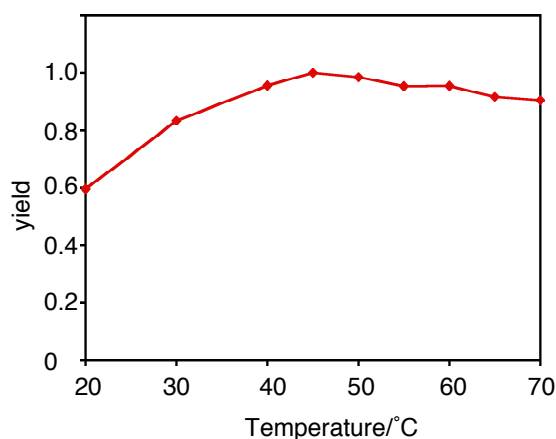


**Figure S3.** The temperature-dependent yields of the ligand exchange reaction. The reactions proceeded for 30 min, [Au] = 0.4 mM, [DppSH] = 8.0 mM.

### (iii) Time course

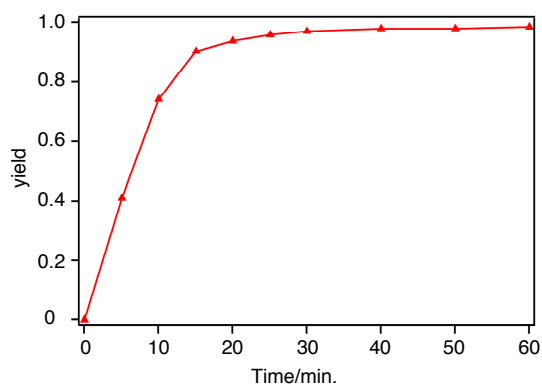


**Figure S4.** The time-dependent yields of the ligand exchange reaction. The reaction proceeded at 50 °C, [Au] = 0.4 mM, [DppSH] = 8.0 mM.

### C. Incubation of Au:SDpp with excess DppSH at 80 °C

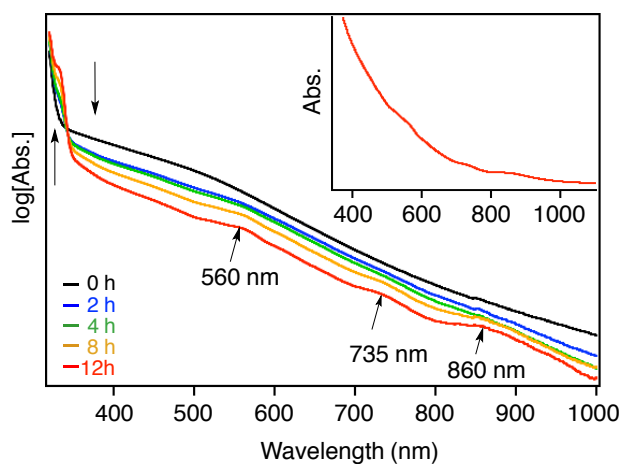


**Figure S5.** Time-course of the UV-vis spectra during incubation of as-extracted Au:SDpp with excess DppSH at 80 °C. The inset shows the UV-vis spectrum obtained after 12 h.

## D. MALDI mass analysis of as-extracted Au:SDpp

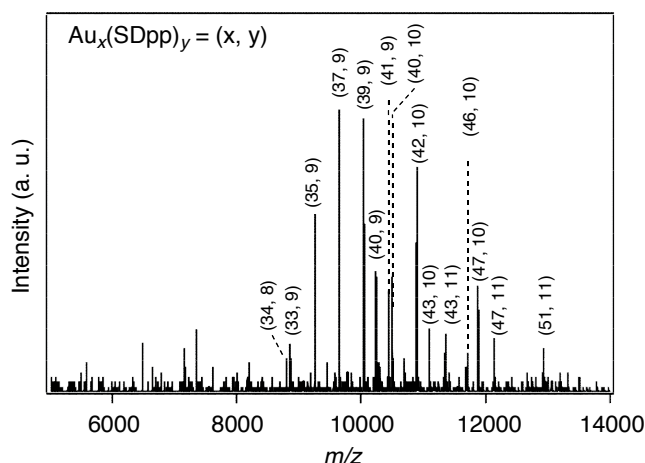


**Figure S6.** MALDI-TOF mass spectrum of as-extracted Au<sub>x</sub>(SDpp)<sub>y</sub> together with tentative assignments.

## E. Incubation of Au:SDpp with excess DppSH at 50 °C

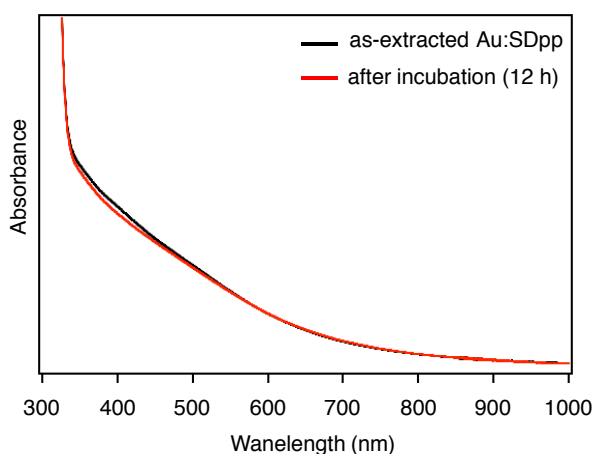


**Figure S7.** UV-vis spectra of as-extracted Au:SDpp and after incubation at 50 °C for 12 h.

## F. MALDI mass analysis of size-focused Au:SDpp

### (i) Laser power dependence

At first, the low-resolution MALDI mass spectra of the size-focused Au:SDpp were recorded in the positive ion mode, which exhibited two peaks at *m/z* of ~7796 and ~7535. The dependence on the relative intensity on laser power showed that the latter corresponds to a parent species, whereas the former corresponds to a photofragment species.

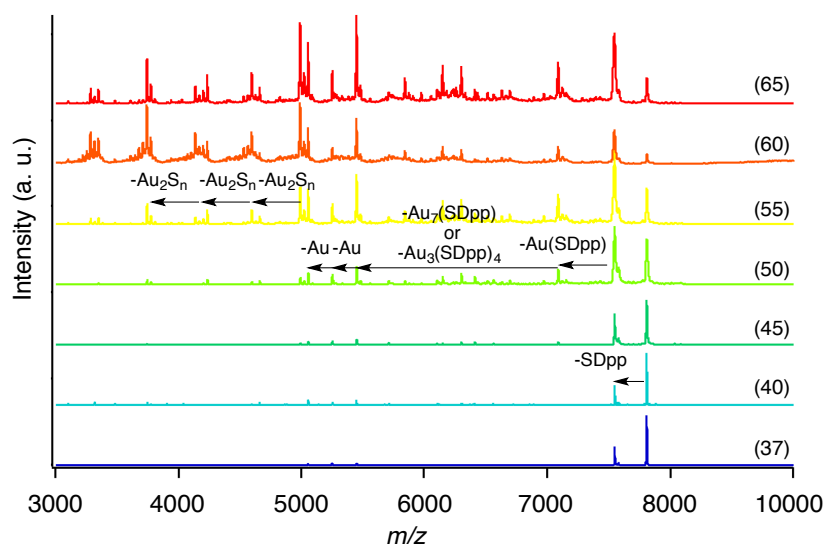


**Figure S8.** MALDI mass spectra of size-focused Au:SDpp recorded at various laser powers. Values in parentheses represent the laser power in arbitrary units.

## (ii) Mass assignment

The size-focused Au:SDpp clusters were assigned using high-resolution MALDI mass spectrometry. We calibrated the mass spectra using monoisotopic signals of the parent and fragment ( $Au_{21}(SC_{12}H_{25})_{14}$ ) of  $Au_{25}(SC_{12}H_{25})_{18}$  as an internal standard. After calibration, the isotope pattern of the parent peak at  $m/z = 7795.8$  was compared with those calculated for several candidates, such as  $Au_{21}(SDpp)_{14}$ ,  $Au_{25}(SDpp)_{11}$ , and  $Au_{29}(SDpp)_8$  (Figures S9a–c). The comparison leads us to assign the parent unambiguously to  $Au_{25}(SDpp)_{11}$ . Similar analysis shows that the fragment peak at  $m/z = 7534.6$  is assigned to  $Au_{25}(SDpp)_{10}$ .

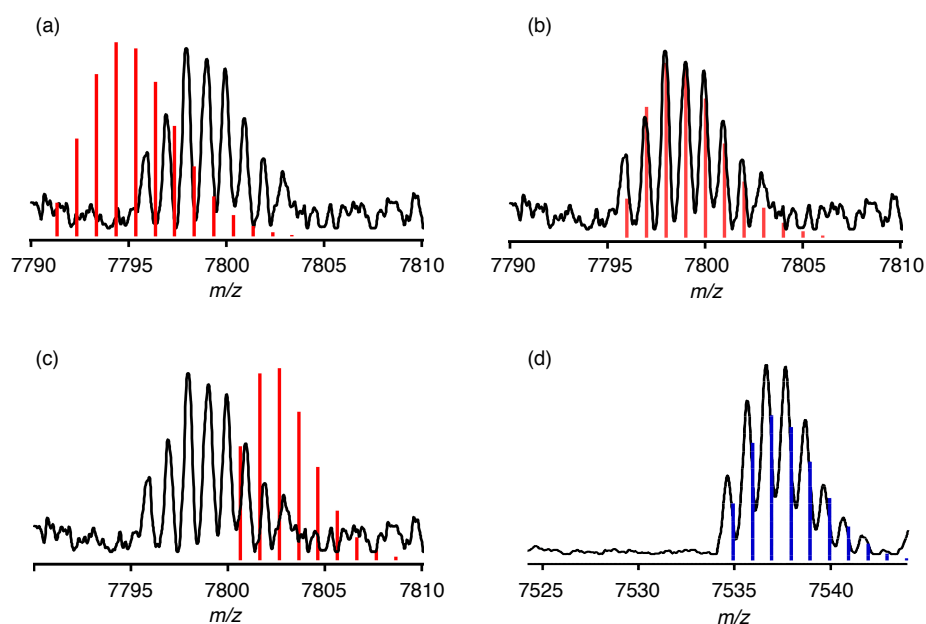


**Figure S9.** The expanded MALDI mass spectra of (a)-(c) parent and (d) fragment signals of size-focused Au:SDpp with simulated isotope patterns of candidates. The bars show simulated isotope patterns of (a)  $Au_{21}(SDpp)_{14}$ , (b)  $Au_{25}(SDpp)_{11}$ , (c)  $Au_{29}(SDpp)_8$ , and (d)  $Au_{25}(SDpp)_{10}$ .

### (iii) Charge state dependence

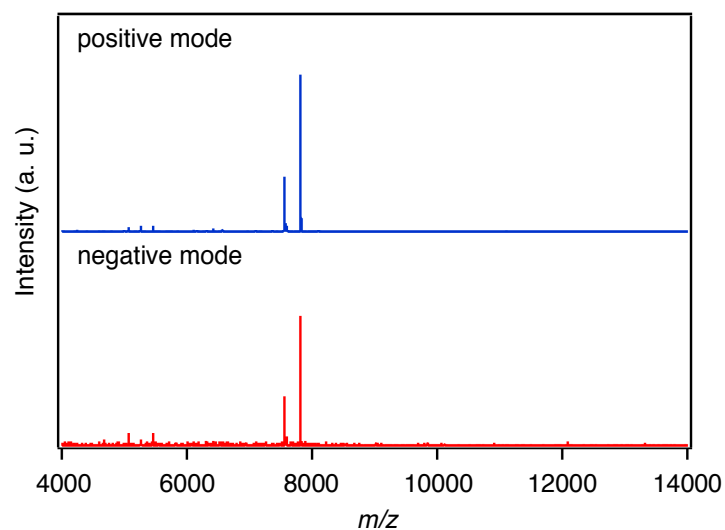


**Figure S10.** MALDI mass spectra of Au<sub>25</sub>(SDpp)<sub>11</sub> recorded in positive and negative mode, respectively.

## G. Characterization of Au<sub>25</sub>(SDpp)<sub>11</sub>

### (i) TEM observation

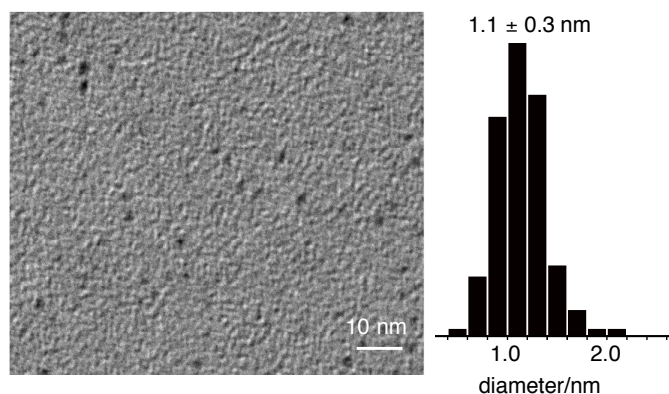


**Figure S11.** Typical TEM image, size distribution of Au<sub>25</sub>(SDpp)<sub>11</sub>.

### (ii) FT-IR spectroscopy

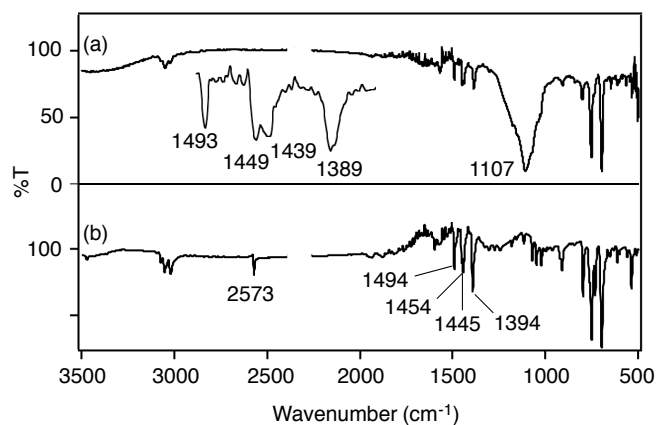


**Figure S12.** IR spectra of (a) Au<sub>25</sub>(SDpp)<sub>11</sub> and (b) DppSH.

### (iii) HEXRD measurement

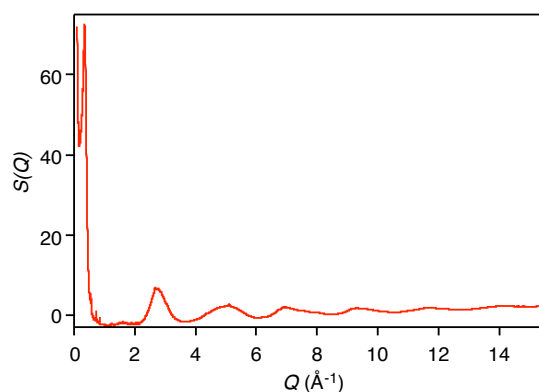


**Figure S13.** The Faber-Ziman total structure factor  $S(Q)$  of  $\text{Au}_{25}(\text{SDpp})_{11}$  obtained from HEXRD measurements.

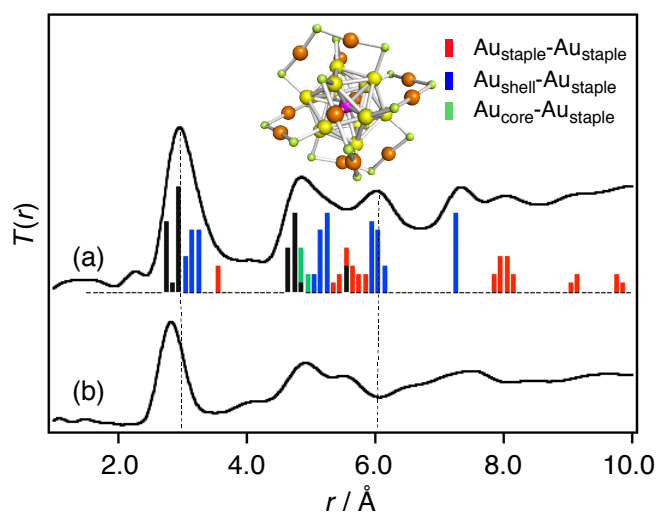


**Figure S14.** Total correlation function  $T(r)$  of (a)  $[\text{Au}_{25}(\text{SC}_2\text{H}_4\text{Ph})_{18}]^-$  and (b)  $\text{Au}_{25}(\text{SDpp})_{11}$  obtained from HEXRD measurements. The histogram in (a) shows the Au-Au distance distribution from crystallographic analysis of  $[\text{Au}_{25}(\text{SC}_2\text{H}_4\text{Ph})_{18}]^-$ . The typical  $\text{Au}_{\text{staple}}\text{-Au}$  bonds in  $[\text{Au}_{25}(\text{SC}_2\text{H}_4\text{Ph})_{18}]^-$  are shown below.

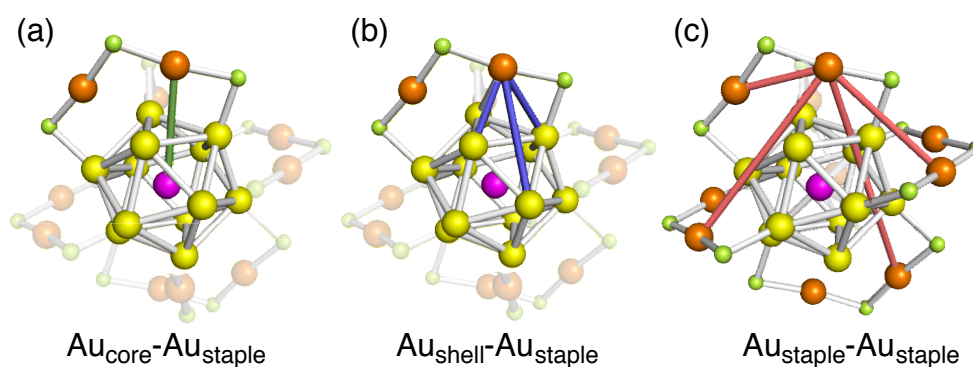


**Figure S15.** Typical  $\text{Au}_{\text{staple}}\text{-Au}$  bonds in  $[\text{Au}_{25}(\text{SC}_2\text{H}_4\text{Ph})_{18}]^-$ .

## References

- 1) Bishop, P. T.; Dilworth, J. R.; Nicholson, T.; Zubieta, J. *J. Chem. Soc., Dalton Trans.* **1991**, 385.
- 2) Tsunoyama, T.; Tsukuda, T. *J. Am. Chem. Soc.* **2009**, *131*, 18216.
- 3) Dass, A.; Stevenson, A.; Dubay, G. R.; Tracy, J. B.; Murray, R. W. *J. Am. Chem. Soc.* **2008**, *130*, 5940.
- 4) Kohara, S.; Itou, M.; Suzuya, K.; Inamura, Y.; Sakurai, Y.; Ohishi, Y.; Takata, M. *J. Phys.: Condens. Matter* **2007**, *19*, 506101.
- 5) Faber, T. E.; Ziman, J. M. *Philos. Mag.* **1965**, *11*, 153.